HISTORICAL EARTHQUAKE SEQUENCES

Larry J. Burdick
Seismological Laboratory 252-21
California Institute of Technology
Pasadena, CA 91125
Tel. (818) 395-6950
Fax (818) 564-0715

(formerly: Woodward-Cyde Consultants
566 El Dorado Street, Suite 100
Pasadena, CA 91101
Tel. (818) 499-7650
Fax (818) 449-3536)

Summary

A rudimentary seismic network has existed in the United States since the mid 1920's. Many important earthquakes in mid-size range ($5 < M < 6$), have been recorded by the relatively low gain instruments from this network, Galitzin's and Wood-Anderson torsions. Because the networks were so sparse, they have not been effectively used. In this report, we have examined records collected form the 1946 Walker Pass and 1947 Manix events and conducted a pilot study into how these records can be used in conjunction with modern data to understand the characteristics of these historic events.

One well-proven method for assessing old events is to compare existing historic recording with observations from modern events (calibration event). The 1962 Walker Pass event ($M_L = 4.9$) was studied in detail for this purpose and observations at Pasadena (PAS) and Florisent (FLO), Missouri compared with the 1946 mainshock and foreshock ($M_L = 5.2$). This comparison yields a $M_O = 1.2 \times 10^{25}$ for the main event with the foreshock estimate lower by about a factor of 3 to 5. The mechanisms do not seem to be the same but all three events are

relatively deep. A comparison of these events with the Manix event recorded at these two stations as well as at Weston, MA indicate that the Manix event is considerably larger.

A detailed modeling effort was conducted on the (PAS) local strong motion recordings of the events separately and in conjunction with the bodywaves recorded at FLO. Considerable effort was devoted to calibrating the upper-mantle model needed in generating the synthetics at FLO. Our best estimate for the Walker Pass mainshock is that it had a strike, dip, and rake of (0°, 40°, 70°) with a moment of 1.5 x 10^{25} ergs, and occurred at a depth of 20 km. Results for the Manix event proved similar to those reported by Doser (1990); essentially a strike-slip event with (65°, 85°, 8), a moment of 3.5 x 10^{25} ergs and a depth of 6 km.

Introduction

The science of seismology has burgeoned in recent decades along with the growth of advanced numerical processing technologies. The growth of these technologies has not slowed in recent times, rather it has accelerated. Yet while processing and analysis technologies improve, the irreplaceable historical seismic data which they could be applied to is constantly being lost. It is stored in the form of simple paper records which are discarded, misfiled or simply decay with time. Earthquakes in a significant tectonic system typically occur decades apart, so associations between tectonic structures and earthquakes must be based on analyses of both these old paper records and modern digital recordings. The purpose of this report is to utilize these significant new analytical methods and technologies in data processing to take advantage of some of these historical data sets and, hopefully, demonstrate their usefulness.

The specific advanced methods we are referring to are new from both a data processing and a data analysis standpoint. Yet they have been proven to be reliable in recent times and there is no reason that they should not be used to both preserve and to make the maximum use of the historical data base. The data processing technology we propose to take advantage of is an automated scanning digitizer which can be used to rapidly and objectively digitize historically significant paper records.

A rudimentary seismic network has existed in California since the mid 1920's. Much of the early data collection was carried out by the Seismological Laboratory of the California Institute of Technology in the southern portion, while the Seismographic Station of the University of California at Berkeley handled the northern portion. Figure 1 is a map showing the location of most of the important events occurring in Southern California since 1932 located by these networks.

These events are obviously related to the tectonic boundary between the North American plate and the Pacific plate which is usually considered to be the San Andreas fault. The San Bernardino Mountains and the associated thicker crust considered to be firmly attached to the North American plate have played a prominent role in deflecting microplates to the West. Thus, the recent activity on the eastern side of the San Andreas (Landers sequence), is adding some excitement. Nur (through personal communication) thinks that new faults are forming along a more northerly direction, essentially the Eastern California Stress Zone. For example, he points out that the Manix event (1947) was interpreted by Richter (1958) to be on a northwest striking fault rather than the conjugate plane to the northeast as indicated on most fault maps. This event has been recently addressed by Doser (1990) and will be studied in this report. Another important event along this zone is the 1946 Walker Pass earthquake sequence which we will also discuss.

The Walker Pass region experienced a M_L = 5.2 foreshock followed by a M_L = 6.3 mainshock 28 minutes later on March 15, 1946. Figure 2a displays the low-gain recordings produced by these events. These events occurred in a region that has not had much activity until recently, starting with the Ridge Crest sequence which is 40 km to the east and presently in progress. The eastern Sierra frontal fault system, as outlined at the top of figure 1, is not well defined at its southern end although it experienced a magnitude 7.7 event in 1872 which apparently produced a right lateral rupture of 6m. The 1946 event occurred at a depth of 22 km as reported by Richter (1958), but its fault parameters have never been determined. Some events

to the east, Durwood Meadows, appear to have extensional tectonics, as reported by Jones and Dollar (1986).

The Manix event occurred on April 10, 1947 and was studied originally by Richter (1958), and more recently by Doser (1990). The $M_L = 6.2$ event produced left-lateral movement on the Manix fault which strikes N70°E at this location. However, the aftershocks appear to be along the conjugate plane, N30°W, as mentioned earlier. A similar phenomenon occurred during the Big Bear sequence according to Jones and Hough (1993).

The strong motions recorded for this event are somewhat larger than those from the Walker Pass event as displayed in figure 2b. The distances are comparable, roughly 180 km. The gains of these instruments are four with a reasonably broadband response, essentially a Long-Period Wood-Anderson torsion instrument. Its properties have been discussed at length by Thatcher and Hanks (1979) with its delta-function response displayed in figure 3, wa.torsion.lp. The high-gain version has a gain of 460 which proves excellent for aftershock studies as they demonstrate. Another excellent instrument that has recorded these old events is the Galitzin. Its response is quite similar to the long-period WWSSN as displayed in figure 3. Excellent Galitzin recording of California events exist at De Bilt, Netherlands, and have been used by many researchers, see Bakun and McEvilly (1984). The gains of these instruments range from about 300 to 800. Other instruments commonly used historically are the Weicherts and Bosch-Omori's, see Helmberger et al., (1992). Galitzin records obtained from the Florisant (FLO) Missouri Station for the Walker Pass and Manix events are displayed in figure 4. Although they are of high quality, they are at upper-mantle triplication distances and difficult to easily interpret.

Only a few teleseismic records exist for the Manix event as discussed by Doser (1990). One of the best set of recordings were written by the Weston Observatory as displayed in figure 5. The Manix event is roughly three times larger than the 1946 mainshock event on all three components. The body wave phases for the 1946 events are too weak to work with unfortunately. The SH body phase for the Manix event as indicated is appropriate for a shallow strike-slip as modeled by Doser (1990). Since teleseismic modeling of body waves is well

developed, we will concentrate our efforts on the local and regional records, that is PAS and FLO.

Event Calibration

One well-proven method for assessing old events is to compare existing historic data with modern data from an event in the same location, see Bent and Helmberger (1991a) for example. We chose the September 1962 event (M_L = 4.9) for this purpose. Both events are located on the eastern edge of the southern Sierra Nevada mountains at approximately 35-75°north and 118°west. P_{nl} modeling of the WWSSN and LRSM data for the 1962 event is displayed in figure 6. The inversion procedure is relatively simple in that only a single crustal layer is needed to model these long-period P_n and P_L waves at ranges 400 to 1200 km, see Wallace and Helmberger (1982). The WWSS stations include BKS, DUG, and ALQ. Only Station PLM (Palomar) existed during 1962 before the station GSC, and Goldstone was established and may not have been calibrated as well as the other stations. From the excellent station coverage we can easily recover the fault orientation and moment as given in the figure. However, the depth cannot be determined by this method, and we use the teleseismic data for this purpose as displayed in figure 7. The depth phases pP and sP become quite apparent, and the depth can be well constrained. The epicentral depth of 16 km is obtained, which is significantly deeper than listed in seismicity reports, Hileman et al., (1973).

This event appears to be relatively high stress drop (Duration = .8 sec with its Moment $M_O = .65 \times 10^{24}$) compared to other Southern California events, Bent and Helmberger (1991b). We can now use the recording of this event at PAS and FLO to compare directly with those from the 1946 events and theoretical predictions.

Modeling Local Seismograms

As recently reported by Dreger and Helmberger (1993), there are remarkable similarities between synthetics generated from a standard Southern California model and waveforms recorded on TERRAscope, a broadband station array. The wide dynamic range of these systems

provides data for the studies of both small and large earthquakes from a given region which allows the isolation of source and propagational features. They find that only one three-component record can be enough to establish source parameters in many situations.

The general procedure is to generate Green's functions for the three fundamental fault types; strike-slip (SS), dip-slip (DS), and 45°dip-slip (45.DS). These functions are then combined linearly with weighting determined by an assumed set of fault parameters to produce a set of synthetic seismograms. The amplitude is determined by the moment. Figure 8 displays a set of predictions assuming a source depth of 8 km, a moment of 1. x 10^{25} dyne-cm, and the standard Southern California model. The motions across each set of traces is normalized to the SS tangential motion on the left. Note that the peak motions decay at a rate slightly less than the distance. Sets of these Green's functions as a function of depth are stored and used to fit observations in a routine fashion, for example see Dreger and Helmberger (1990).

More recent modeling attempts, Zhao and Helmberger (1994), indicate that whole seismograms can be used in source estimation with less difficulty by applying a "cut and paste" approach. By applying this method, we compare portions of the synthetics to the data so that the precise timing between the first arriving P_{nl} portion and the later arriving S-wave is not necessary. Figure 9a displays the modeling of the September 16, 1962 event as recorded at PAS applying this method. Note that the beginning P-wave portion, P_{nl}, has been removed and aligned to the corresponding observations. The best fitting source model denoted by strike, dip, and rake is then obtained by least-squared waveform modeling determined by a direct grid search, see figure 9b. The upper panel displays the fit predicted from the teleseismic and regional modeling study. The results are in reasonable agreement and probably yield about the expected accuracy using just a standard model.

Results for the 1946 event are displayed in figure 10. The lower panel gives the solution based on the grid search while the upper panel shows the fits obtained from modeling the FLO data as displayed in figure 4 and discussed in the next section. These solutions are similar to the 1962 event but with a stronger strike-slip component.

The Manix event appears to be larger teleseismically as discussed earlier, and this proves true locally as well. Figure 11 displays these results with the inversion at the bottom and Doser's solution assumed in the upper panel. The moments agree but the mechanism is quite different. Solutions obtained from modeling the FLO data prove to be in agreement with both as discussed next.

Modeling Upper-Mantle Records

Tangential component (SH polarized) seismograms from over 100 events located in the western United States, Gulf of California, and the East Pacific Rise have been studied in detail with respect to upper-mantle structure, see for example, Grand and Helmberger (1984), and Grand (1994) for 1-D regionalizations and 2-D structures in Helmberger et al., (1985). The earthquakes selected were generally strike-slip and only seismograms at the maximum SH radiation patterns were used.

The SH waveform from a strike-slip earthquake does not change much with azimuth except at its nodes. This is easily seen in observed motions as displayed in figure 12. This figure compares observations from the Truckee earthquake with synthetics. Two sets of synthetics are displayed with the top set corresponding to a depth of 16 km and the bottom set for a depth of 14 km. The numbers following the synthetics indicate the moments required to fit that particular seismogram. The amplitudes of the data are given in (cm) x 10^{-3} with the instrumental gain removed. Most of these records are small, only a few cm on the original records. Nevertheless, the surface reflecting sS is very clear along the maximum loop near the station GWC. As one approaches the node, the amplitude ratio of sS/S becomes quite sensitive to the dip and rake and causes waveform instabilities, see Burdick and Mellman (1976). Away from the node, one sees a quite stable behavior in amplitude with SCH being the most anomalous but still less than a factor of two off. It appears that this level of accuracy is also possible at upper-mantle ranges as demonstrated in figure 13. Note that we have omitted the amplitude of the nodal LRSM station (RKON). The SH motions here were modeled assuming a source depth of 4 km, a pure strike-slip earthquake and the 2-D RMFM (Rocky Mountain Front Model), Helmberger et al., (1985).

A t^* of 3.0 was assumed in this calculation and sS cannot be distinguished from S at these periods. The triplications are particularly obvious at ranges less than 19° (400 km triplication) and between 24 to 28° (600 km triplication). The waveforms are quite simple near 22°. The synthetic at FLO has a problem in that the Green's function is too sharp and the moment estimate has the largest error, a factor of three too large. Removing some of the high frequency would help solve this disparity but, in general, the amplitudes of the synthetics fit the observations very well.

The situation for P is not quite so good in that the PP-P waveforms are quite complicated as reported recently, Lefevre and Helmberger (1989). Thus, we will rely on the P-wave study by Burdick and Helmberger (1978) and use their T7 upper-mantle model. This 1-D model maps the lateral variation of slow TNA (Tectonic North America) into the vertical structure to account for the SNA (Stable North America) bias. This was caused by using west coast sources and east coast stations. However, this model fits the P-waves better than assuming RMFM and a constant Poisson's ratio.

a) Walker Pass (1962) event

It would be good to check the above models against the 1962 Walker Pass data at FLO but this proved difficult. The problem is noise at these low magnitudes. These records were scanned, processed, and replotted in figure 14. The reproduction looks better than the original but probably suspect in detail. But it appears that the ratios of SV (WE) to SH (SN) to P (Z) are similar to the 1946 foreshock. The SV waveforms are identical and differ in amplitude by a factor of 18. This comparison yields a moment estimate of 1.2×10^{25} ergs. We think the noise is too large to model the P and SH waveforms. The SV waveforms are always difficult to model because of the well-known S-PL problems, see Helmberger and Engen (1980). Fortunately, the long-period world-wide station was just starting operation with its vertical record displayed in the bottom trace of figure 14. An enlargement of the P-wave is given in figure 15 along with a synthetic prediction. Actually the FLO record was written by a (30,90) instead of the current

(15,100) which accounts for the slightly longer tail portion. The horizontal components were unstable on this particular day and not usable.

b) Walker Pass (1946) event

The P and SH-waveforms from the 1946 Walker Pass foreshock and mainshock have been enlarged from the seismograms presented earlier and displayed in figure 16. The lower half of figure 16 presents the synthetics appropriate for the two mechanisms introduced with respect to modeling the local PAS recording, see figure 11. The top set of synthetics fit quite well since the amplitude ratio of P to SH was obtained by adjusting the fault parameters to produce this match; essentially perturbations of the 1962 mechanism. This moment estimate is 1.5×10^{25} ergs. The bottom set correspond to the solution found by the direct inversion of the PAS records. This solution does not produce a very good match to the P-wave. Note that the foreshock appears to be about one quarter the size of the main event with about the same mechanism. This conclusion is quite compatible with both the PAS and Weston observations.

While there remains some uncertainty about the precise mechanism, the depth appears to be well established, as demonstrated in figure 17. This depth sensitivity test shows the strong waveform dependence on the surface reflected in phase sS. As displayed earlier in figures 12 and 13, the separation of S and sS show a particularly strong interference when the epicentral depths are greater than 15 km, probably near 20 km.

c) Manix (1947) event

The results for the Manix event are presented in figure 18 following the above format. The solution proposed by Doser (1990) in the upper set of synthetics does quite well with the depth set at 6 km. The observed P-wave signal is somewhat more complicated than the synthetic which may be caused by a more complex triplication. The first down swing is produced by energy bottoming at depths near 530 km and appears to be early relative to the synthetic. It is difficult to account for such details but the main three pulses, P, pP, and sP look quite good. The amplitude is slightly large which can be easily fixed by moving the strike to 67°which makes the

P-wave nearly nodal. The SH-wave fit is not very good and may be caused by a secondary event as suggested by Doser (1990). The time history assumed here, trapezoidal shape, was set at (1,1,6) sec as indicated in Doser's one source model.

The prediction from the best fitting synthetics to PAS are given in the bottom set. This solution is not good in that it does not satisfy the SH-polarity and the P-wave is too large. Thus, a solution closer to a pure strike-slip is preferred.

Discussion

A relatively large number of events have now been recorded by TERRAscope, some near sites of historic events. This allows the historic records collected at PAS (1930-1960) on the low gain long-period (6-8 sec-torsions) and short-period (low gain Wood-Anderson) to be directly compared with modern calibration events. Some of the larger events, M>5, can be seen regionally on the old broadband instruments at Berkeley and Florisant (Galitzin's) while still larger events, M>6, can be observed teleseismically (i.e., DeBilt).

To understand these seismograms and separate propagational distortions from source properties is relatively easy at teleseismic distances (Helmberger et al., 1992a), but becomes more difficult at regional and local distances. Fortunately, the digital systems used in the TERRAscope array provide observations that greatly aid in establishing the nature of local wave propagation. For example, the wide dynamic range allows motions from small events (aftershocks) to be compared with large events at the same site even though the motions can differ by several orders of magnitude. Signals at these distances have not suffered mantle attenuation and thus the broadband features of this system allow us to see obvious propagational effects (headwaves and critical reflections) and detailed source characteristics (near-field and source complexity), see Helmberger et al., (1992, 1993).

At upper-mantle distances such as FLO, the propagational corrections are quite complex but appear to be manageable as demonstrated in this report. Thus, we can examine the many events in the $5 < M_L < 6$ class at this station where the signal-to-noise ratio is about 5 times higher than it is teleseismically. The Manix event is near the teleseismic threshold as can be seen

by examining those records presented by Doser (1990). We have examined a few dozen Galitzin records from FLO and found them quite readable. Thus, the combination of local records (PAS and BKS) and FLO should prove highly useful in establishing the nature of the many historic significant events.

References

Hileman, J., C. R. Allen, and J. M. Nordquist (1973). Seismicity of the Southern California Region, January 1, 1932 to December 31, 1972, Seismological Laboratory, California Institute of Technology.

Thatcher, W. and T. C. Hanks (1973). Source Parameters of Southern California Earthquakes, *JGR*, **78**, no. 35, 8547-8576.

Burdick, L. J. and G. R. Mellman (1976). Inversion of the body waves of the Borrego Mountain earthquake to the source mechanism, *Bull. Seism. Soc. Am.*, **66**, 1485-1499.

Burdick, L. J. and D. V. Helmberger (1978). The Upper Mantle *P* Velocity Structure of the Western United States, *JGR*, **83**, no. B4, 1699-1712.

Helmberger, D. V. and G. R. Engen (1980). Modeling the Long-Period Body Waves from Shallow Earthquakes at Regional Ranges, *Bull. Seism. Soc. Am.*, **70**, no. 5, 1699-1714.

Helmberger, D. V., G. Engen, and S. Grand (1985). Upper-mantle cross-section from California to Greenland, *J. Geophys.*, **58**, 92-100.

LeFevre, L. V. and D. V. Helmberger (1989). Upper Mantle *P* Velocity Structure of the Canadian Shield, *JGR*, **94**, no. B12, 17,749-17,765.

Doser, D. I. (1990). A Re-examination of the 1947 Manix, California, Earthquake sequence and comparison to other sequences within the Mojave block, *Bull. Seism. Soc. Am*, **80**, no. 2, 267-277.

Dreger, D. S. and D. V. Helmberger (1990). Broadband Modeling of Local Earthquakes, *Bull. Seism.. Soc. Am..*, **80**, no. 5, 1162-1179.

Bent, A. L. and D. V. Helmberger (1991a). A Re-examination of Historic Earthquakes in the San Jacinto Fault Zone, California, *Bull Seism. Soc. Am.*, **81**, no. 6, 2289-2309.

Bent, A. L. and D. V. Helmberger (1991b). Seismic Characteristics of Earthquakes along the Offshore Extension of the Western Transverse Ranges, California, *Bull. Seism. Soc. Am.*, **81**, no. 2, 319-422.

Helmberger, D. V., P. G. Somerville, and E. Garnero (1992). The Location and Source Parameters of the Lompoc, California, Earthquake of 4 November 1927, *Bull. Seism. Soc. Am.*, **82**, no. 4, 1678-1709.

Helmberger, D. V., R. Stead, P. Ho-Liu, and D. Dreger (1992). Broadband modelling of regional seismograms: Imperial Valley to Pasadena, *Geophys. J. Int.*, **110**, 42-54.

Dreger, D. S. and D. V. Helmberger (1993). Determination of Source Parameters at Regional Distances with Three-Component Sparse Network Data, *J. Geophys. Res.*, **98**, no. B5, 8107-8125.

Jones, L. E., S. E. Hough, and D. V. Helmberger (1993). Rupture Process of the June 28, 1992 Big Bear Earthquake, *Geophys. Res. Lett.*, **20**, no. 18, 1907-1910.

Helmberger, D. V., D. Dreger, R. Stead, and H. Kanamori (1993). Impact of Broadband Seismology on the Understanding of Strong Motions, *Bull. Seism. Soc. Am.*, **83**, no. 3, 830-850.

Zhao, L-S. and D. V. Helmberger (1993). Source Retrieval from broadband regional seismograms: Hindu Kush region, *Phys. Earth Planet. Int.*, **78**, 69-95.

FIGURES

Figure 1. Upper map displays the major fault zones in Southern California along with the location of the major ruptures. The lower map includes the seismicity prior to the Landers earthquake.

Figure 2. Upper panel displays a copy of the 1946 Walker Pass strong motion recordings as observed at Pasadena (gain of 4). The lower panel compares these records with those from the Manix event at comparable distance, 180 km. Peak amplitudes in cm are indicated above each trace.

Figure 3. Instrumental responses of analog instruments commonly employed in the historical dataset, along with their gains and recording speeds. Note the similarity between the Galitzin response and the world-wide long-period (WWSSN.lp) which has been in observation for the last 30 years.

Figure 4. Comparison of Galitzin recordings obtained from FLO for the Manix and Walker Pass events. Peak amplitudes (zero to peak) are indicated above each trace.

Figure 5. Comparison of Weston recordings of the two events on the NS component which are apparently naturally rotated.

Figure 6. Regional observations of the calibration event, 16 September 1962, against synthetics assuming the crustal model discussed in Helmberger and Engen (1978). The numbers above each trace indicate the peak amplitude. Note the excellent fits except the PLM (Radial) which could be a calibration problem. The moment obtained is .65 x 10^{24} ergs.

Figure 7. Comparison of the short-period recordings of this event at teleseismic distances, eastern stations of the LRSM and WWSS networks as indicated in the map. The delay of the phase pP relative to P controls the depth estimate. The amplitude of each trace is indicated assuming the M_O obtained from the P_{nl} fits and adjusting the source time history assumed to be a triangle (.4 sec, .4).

Figure 8. Theoretical profiles of strong motion synthetics (long-period torsion with gain of 4) for the tangential and radial components assuming the three fundamental fault orientations and the standard SC model.

Figure 9. Upper panel displays the fits obtained by assuming the source mechanism determined by the P_{nl} and teleseismic modeling. The lower panel contains the results by applying the source-inversion code directly.

Figure 10. Comparison of the Walker Pass strong motion results assuming a source model (upper) and lower after inversion.

Figure 11. Comparison of the Manix strong motion results assuming the Doser model (upper) and lower after inversion.

Figure 12. Comparison of teleseismic SH-waveform observations of the Truckee earthquake and synthetics. The upper set of synthetics assumes a depth of 14 km while the lower set assumes a depth of 16 km. The numbers behind each observed record indicate the peak amplitude in cm (10^{-3}). The amplitude on the synthetics are estimates of the moment required to fit that particular record.

Figure 13. Comparison of upper-mantle observations with synthetics showing the complexities of triplications, see Burdick and Helmberger (19xx).

Figure 14. The upper three traces are the observations of the 1962 Walker Pass event as obtained from the Galitzin's. The bottom trace contains the vertical component of the WWSSN system where the P and S waves are quite clear.

Figure 15. The middle trace displays a blow-up of the long-period observation (bottom trace in figure 14). The lower trace displays the short-period observation (WWSSN) on the same time scale. The top trace is a synthetic generated by assuming the RMFM, the moment obtained from the Pnl fits and a depth of 16 km.

Figure 16. Comparison of observations and synthetics with amplitude expressed in peak-to-peak values.

Figure 17. Comparison of observed (Walker Pass, 46) and synthetics with various source depths in km.

Figure 18. Comparison of observed P and SH waveforms against two sets of synthetics. Middle (Doser), bottom (from the Pass inversion).

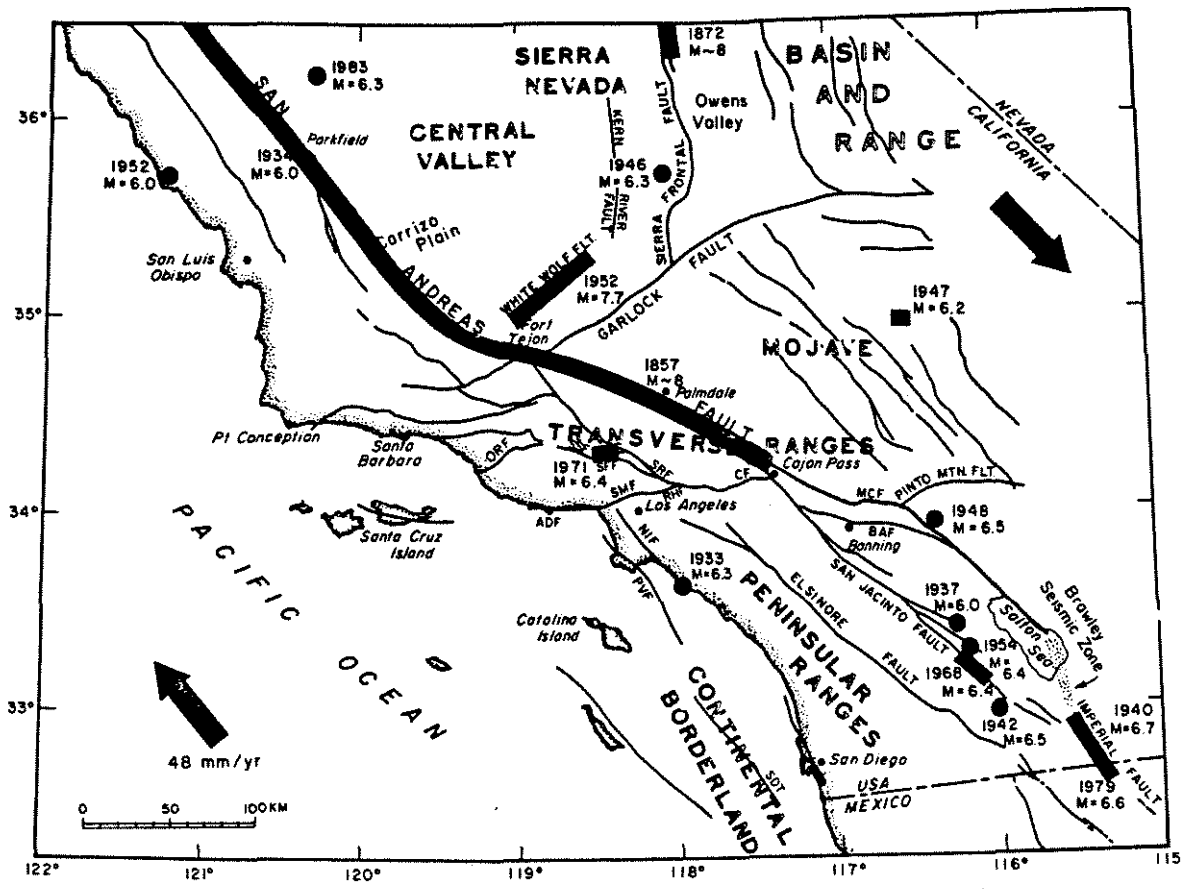
SIERRA NEVADA
BASIN AND RANGE
CENTRAL VALLEY
MOJAVE
TRANSVERSE RANGES
PENINSULAR RANGES
CONTINENTAL BORDERLAND
PACIFIC OCEAN
SAN ANDREAS FAULT
GARLOCK FAULT
SIERRA FRONTAL FAULT
KERN RIDGE FAULT
WHITE WOLF FLT
PINTO MTN FLT
ELSINORE FAULT
SAN JACINTO FAULT
IMPERIAL FAULT
NEVADA CALIFORNIA
Owens Valley
Parkfield
Carrizo Plain
Fort Tejon
San Luis Obispo
Pt Conception
Santa Barbara
Santa Cruz Island
Catalina Island
Los Angeles
Palmdale
Cajon Pass
San Diego
Salton Sea
Brawley Seismic Zone
USA
MEXICO
1872 M~8
1983 M=6.3
1952 M=6.0
1934 M=6.0
1946 M=6.3
1952 M=7.7
1947 M=6.2
1857 M~8
1971 M=6.4
1948 M=6.5
1933 M=6.3
1937 M=6.0
1954 M=6.4
1968 M=6.4
1942 M=6.5
1940 M=6.7
1979 M=6.6
48 mm/yr
0 50 100KM
36°
35°
34°
33°
122°
121°
120°
119°
118°
117°
116°
115°

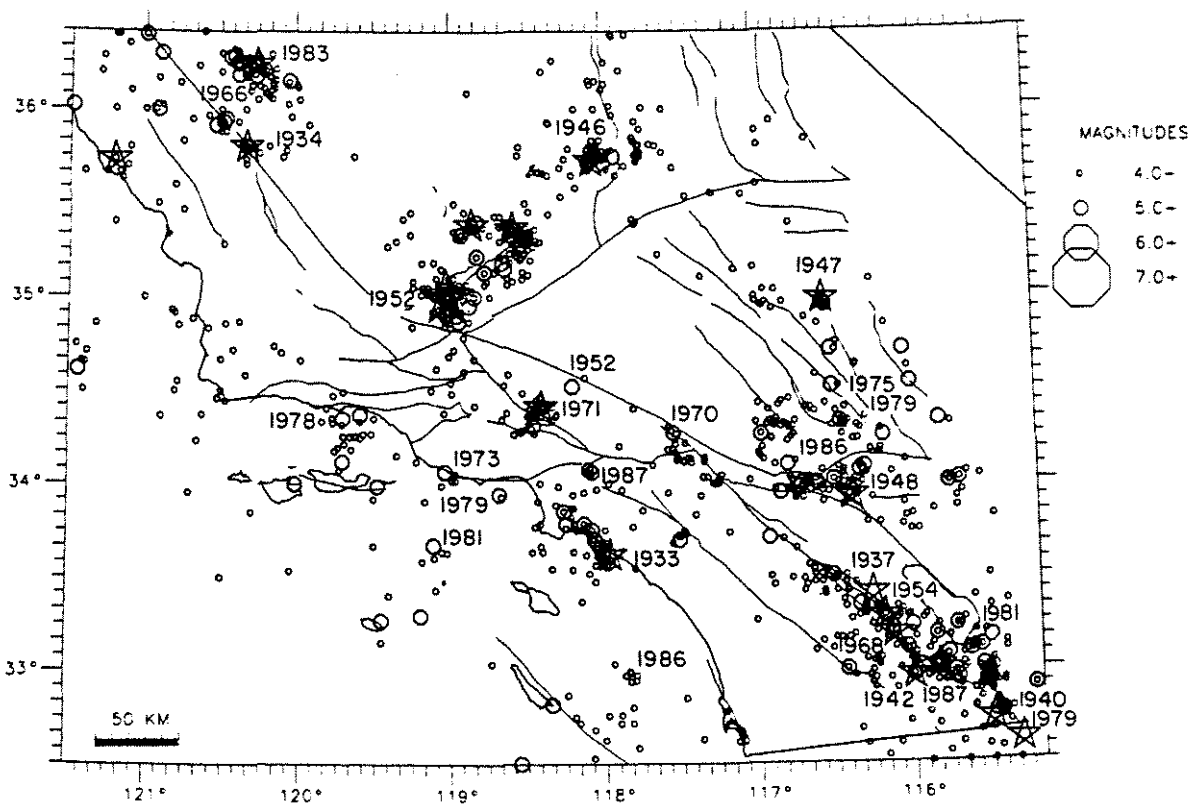
MAGNITUDES
4.0+
5.0+
6.0+
7.0+
50 KM
1983
1966
1934
1946
1952
1947
1971
1978
1970
1975
1979
1986
1973
1987
1948
1981
1933
1937
1954
1968
1942
1940
36°
35°
34°
33°
121°
120°
119°
118°
117°
116°

fig 1

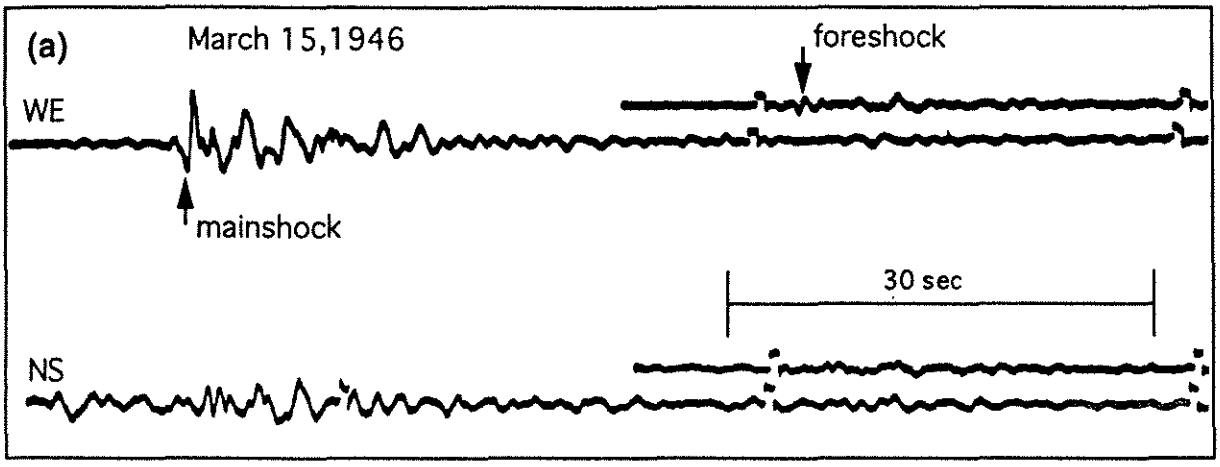
(a)
March 15,1946
foreshock
WE
mainshock
30 sec
NS

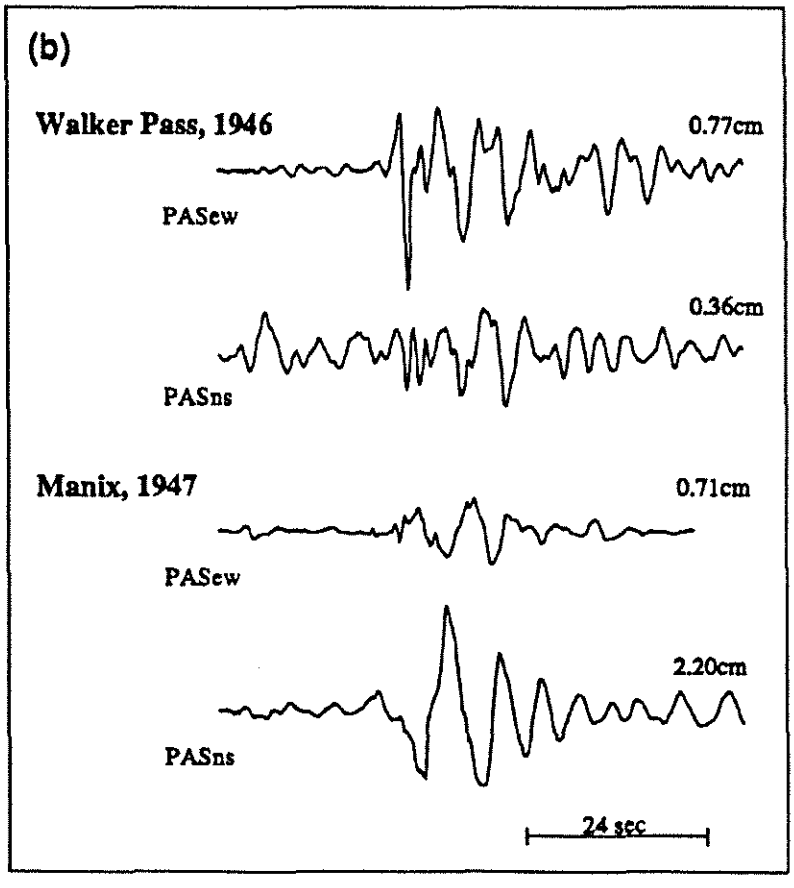
(b)
Walker Pass, 1946
0.77cm
PASew
0.36cm
PASns
Manix, 1947
0.71cm
PASew
2.20cm
PASns
24 sec

fig 2

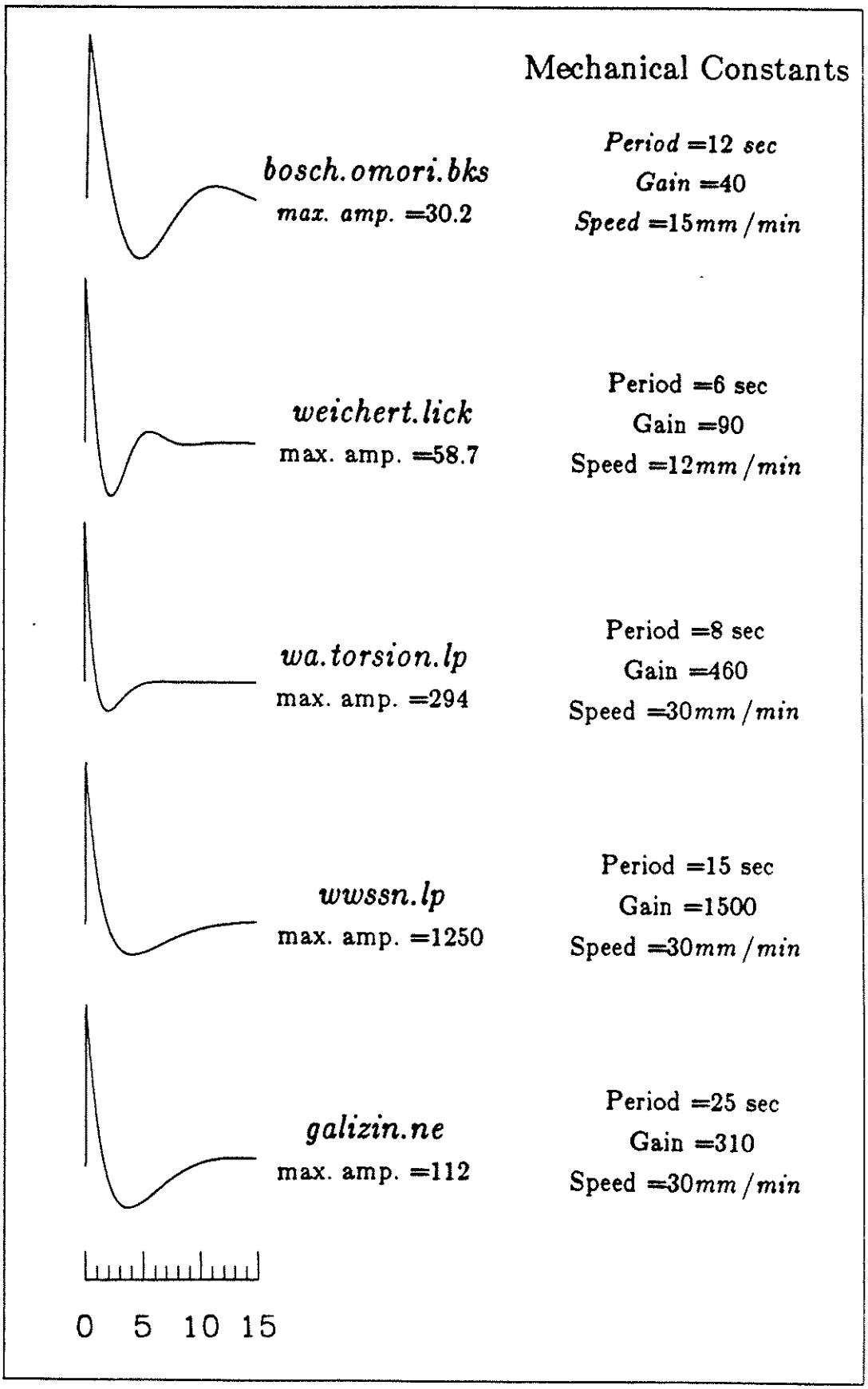
Mechanical Constants
bosch.omori.bks
max. amp. =30.2
Period =12 sec
Gain =40
Speed =15mm/min
weichert.lick
max. amp. =58.7
Period =6 sec
Gain =90
Speed =12mm/min
wa.torsion.lp
max. amp. =294
Period =8 sec
Gain =460
Speed =30mm/min
wwssn.lp
max. amp. =1250
Period =15 sec
Gain =1500
Speed =30mm/min
galizin.ne
max. amp. =112
Period =25 sec
Gain =310
Speed =30mm/min
0 5 10 15

fig 3

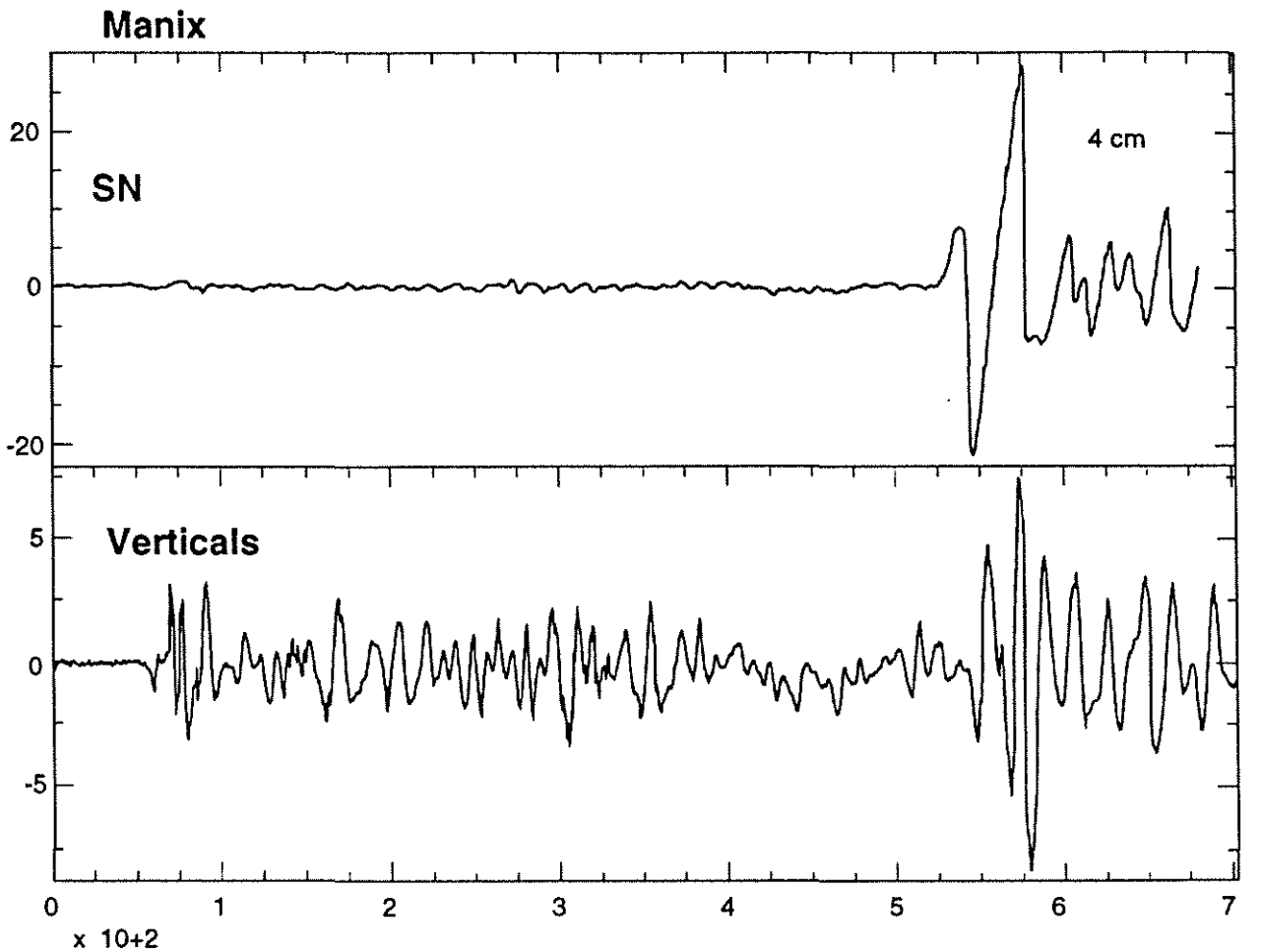
Manix
20
SN
4 cm
0
-20
5
Verticals
0
-5
0
1
2
3
4
5
6
7
x 10+2

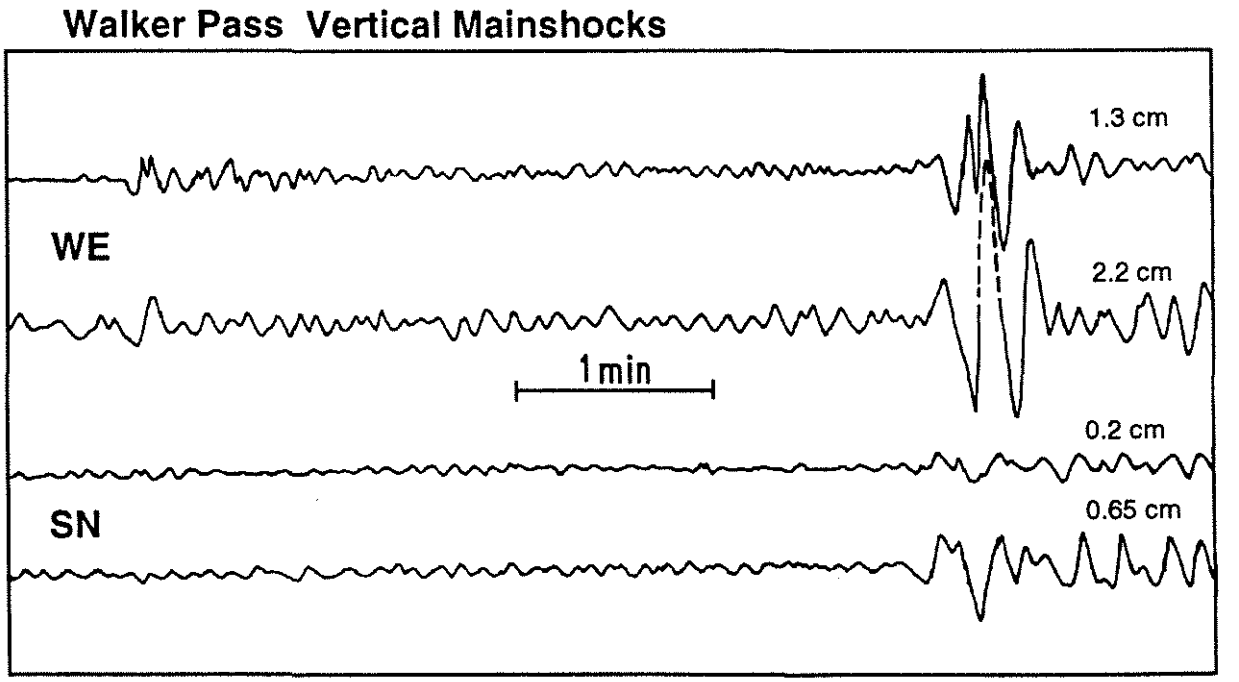
Walker Pass Vertical Mainshocks
1.3 cm
WE
2.2 cm
1 min
0.2 cm
SN
0.65 cm

fig 4

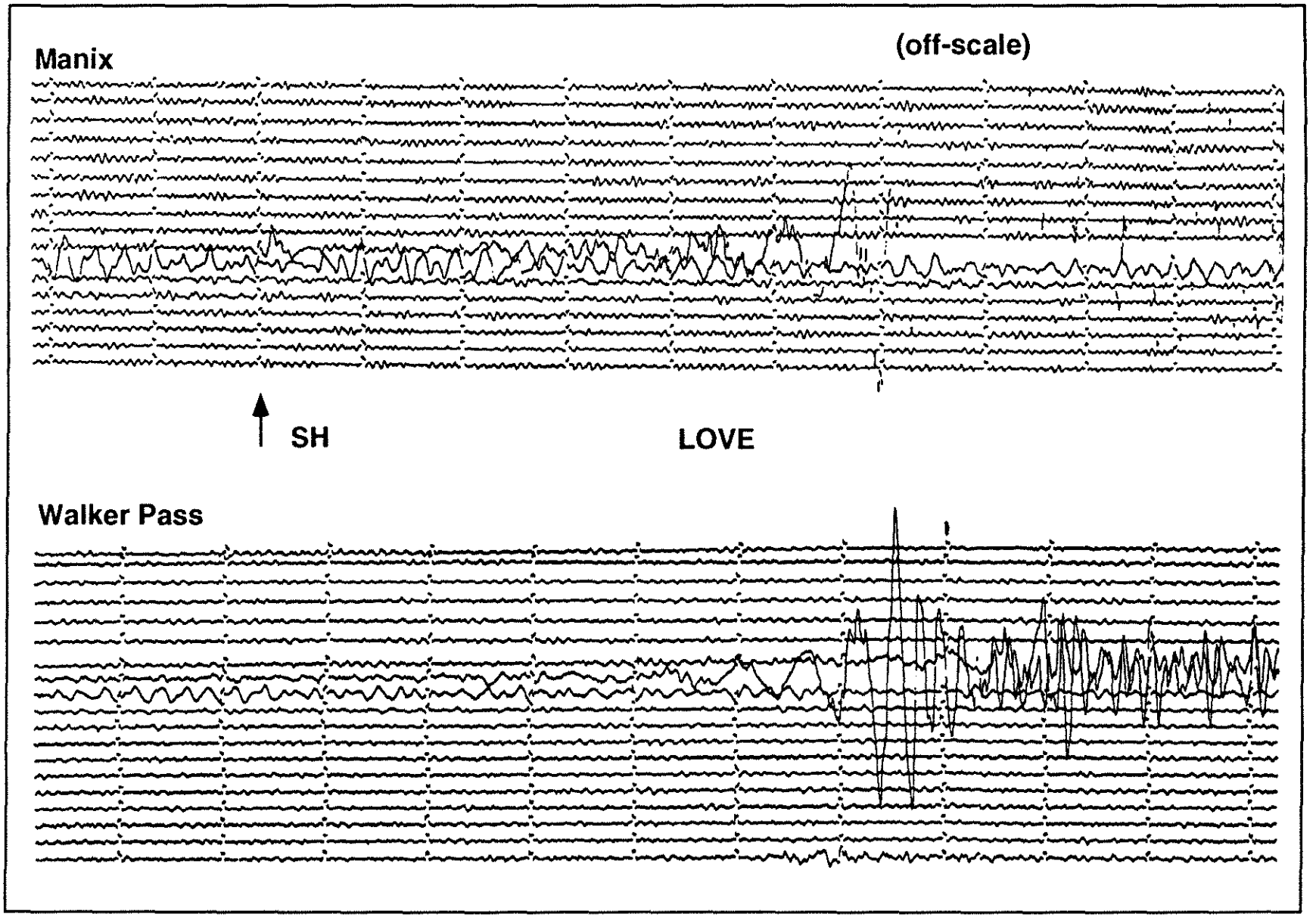

Fig 5

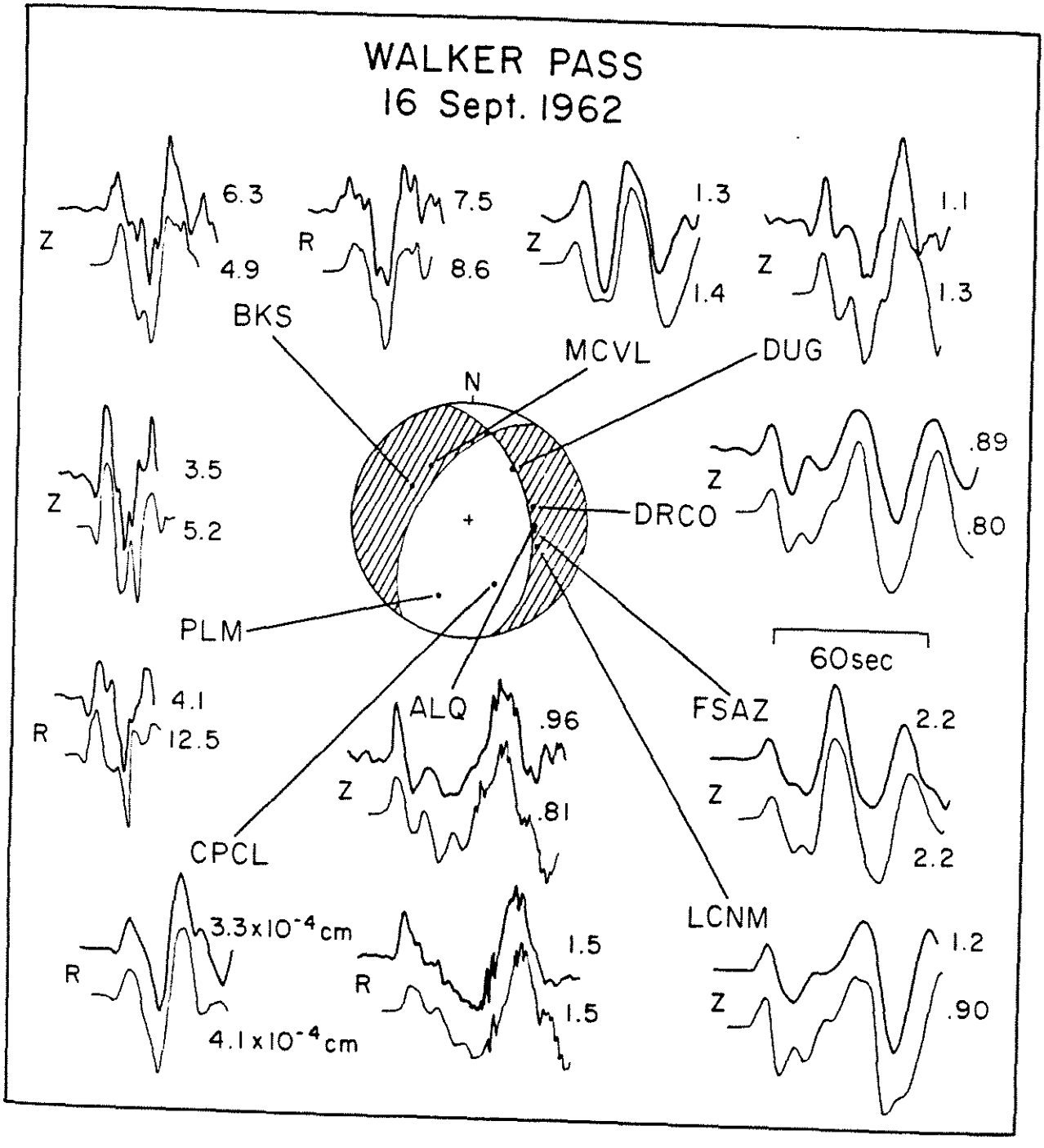
WALKER PASS
16 Sept. 1962
Z
6.3
4.9
R
7.5
8.6
Z
1.3
1.4
Z
1.1
1.3
BKS
MCVL
DUG
N
Z
3.5
5.2
Z
.89
.80
DRCO
PLM
60sec
R
4.1
12.5
ALQ
Z
.96
.81
FSAZ
Z
2.2
2.2
CPCL
R
3.3x10⁻⁴cm
4.1x10⁻⁴cm
R
1.5
1.5
LCNM
Z
1.2
.90

fig 6

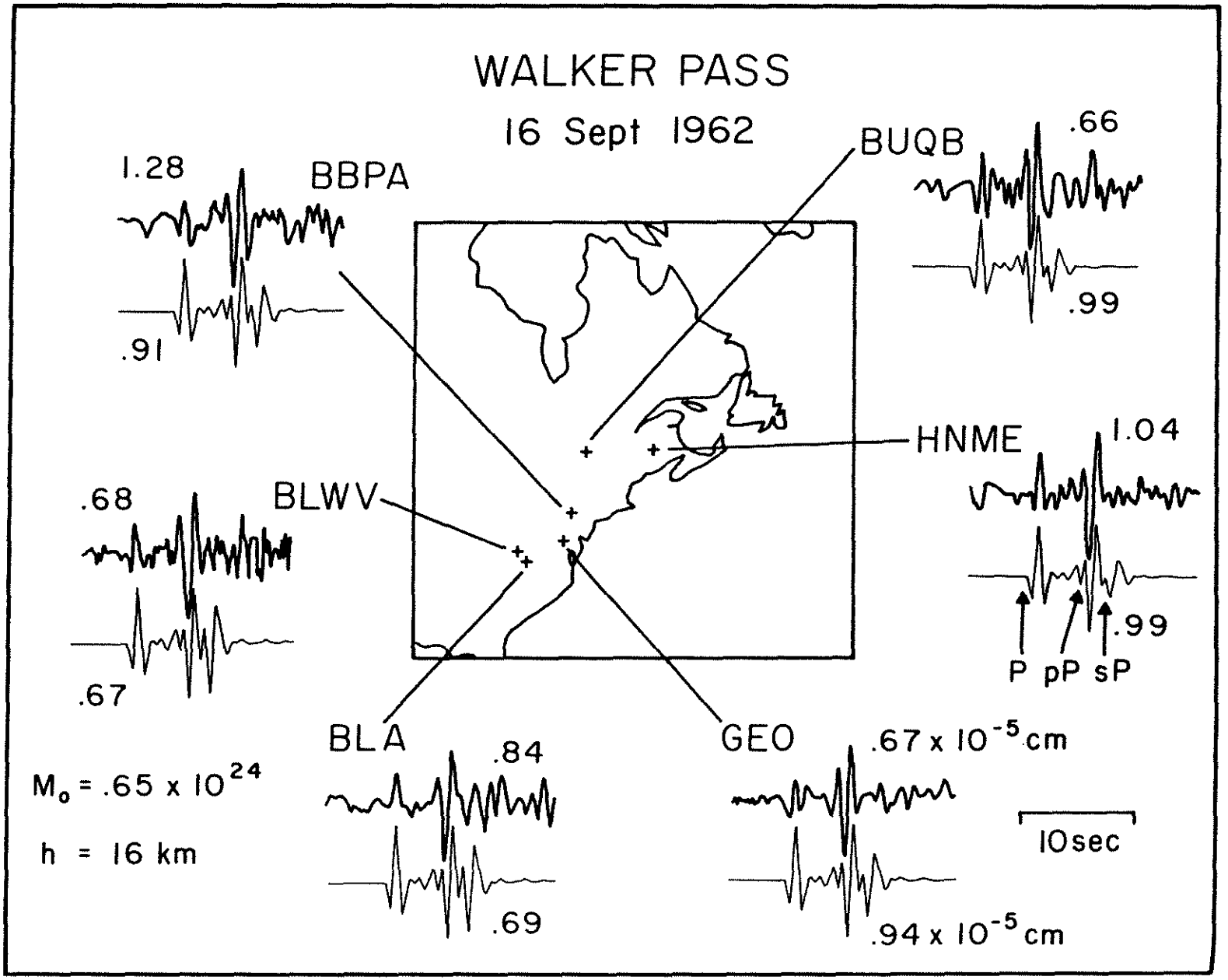
WALKER PASS
16 Sept 1962
1.28
BBPA
.91
BUQB
.66
.99
HNME
1.04
.99
P pP sP
.68
BLWV
.67
BLA
.84
.69
GEO
.67 x 10^-5 cm
.94 x 10^-5 cm
10sec
M0 = .65 x 10^24
h = 16 km

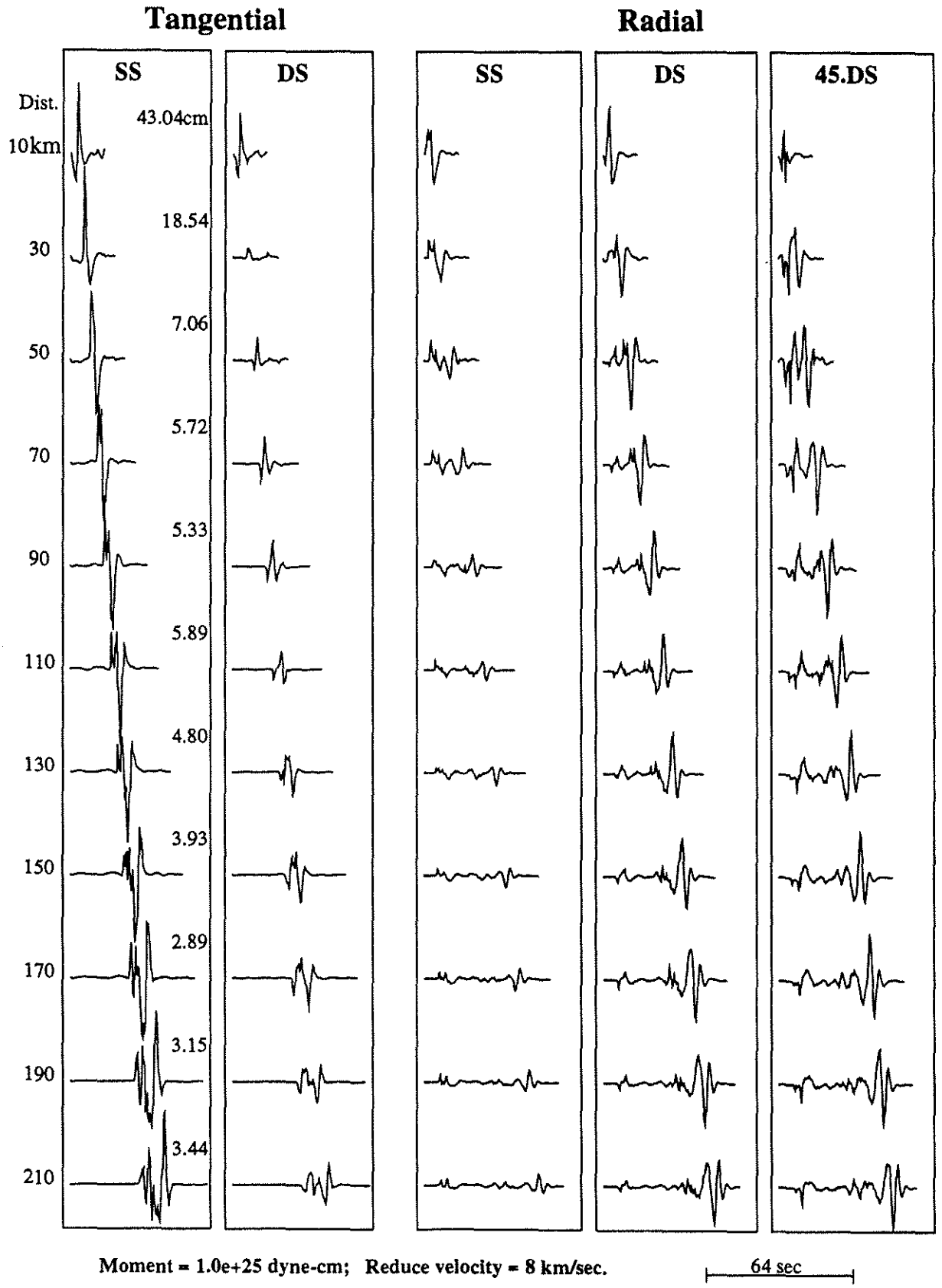

Moment = 1.0e+25 dyne-cm; Reduce velocity = 8 km/sec.

64 sec

fig 7

fig 8

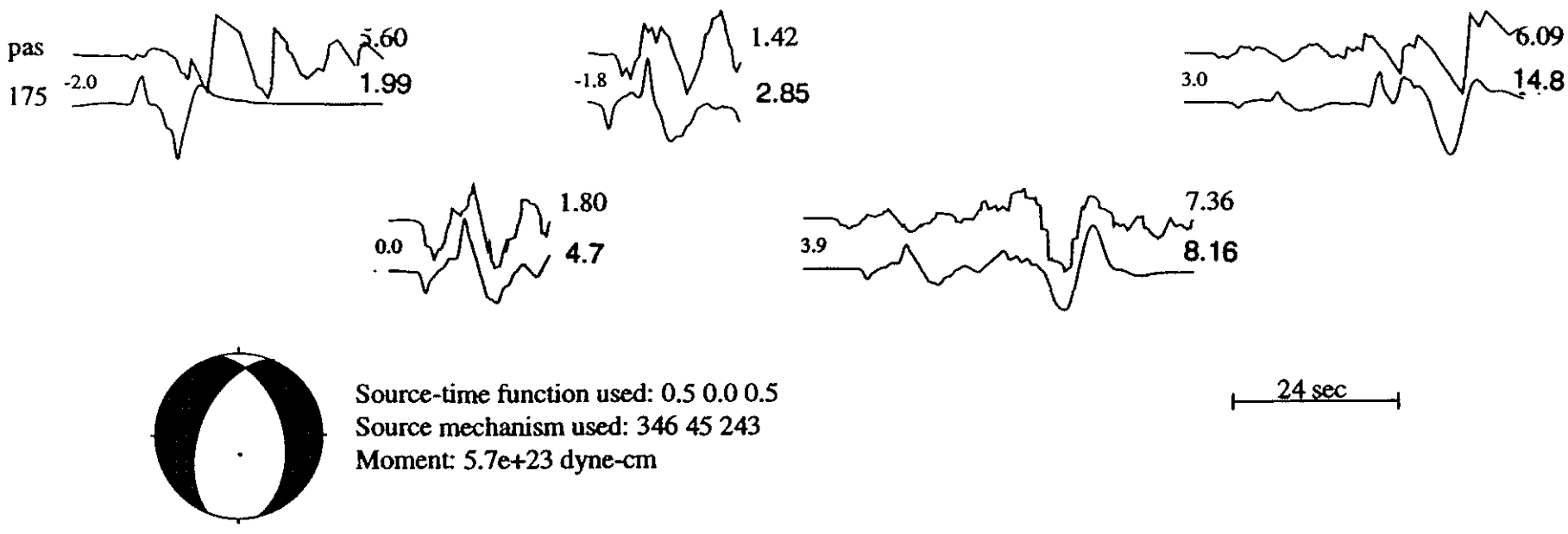
Tangential
Rad. Pnl
Ver. Pnl
Rad. Whl.
Ver. Whl.
pas
175
-2.0
5.60
1.99
-1.8
1.42
2.85
3.0
6.09
14.8
0.0
1.80
4.7
3.9
7.36
8.16
Source-time function used: 0.5 0.0 0.5
Source mechanism used: 346 45 243
Moment: 5.7e+23 dyne-cm
24 sec

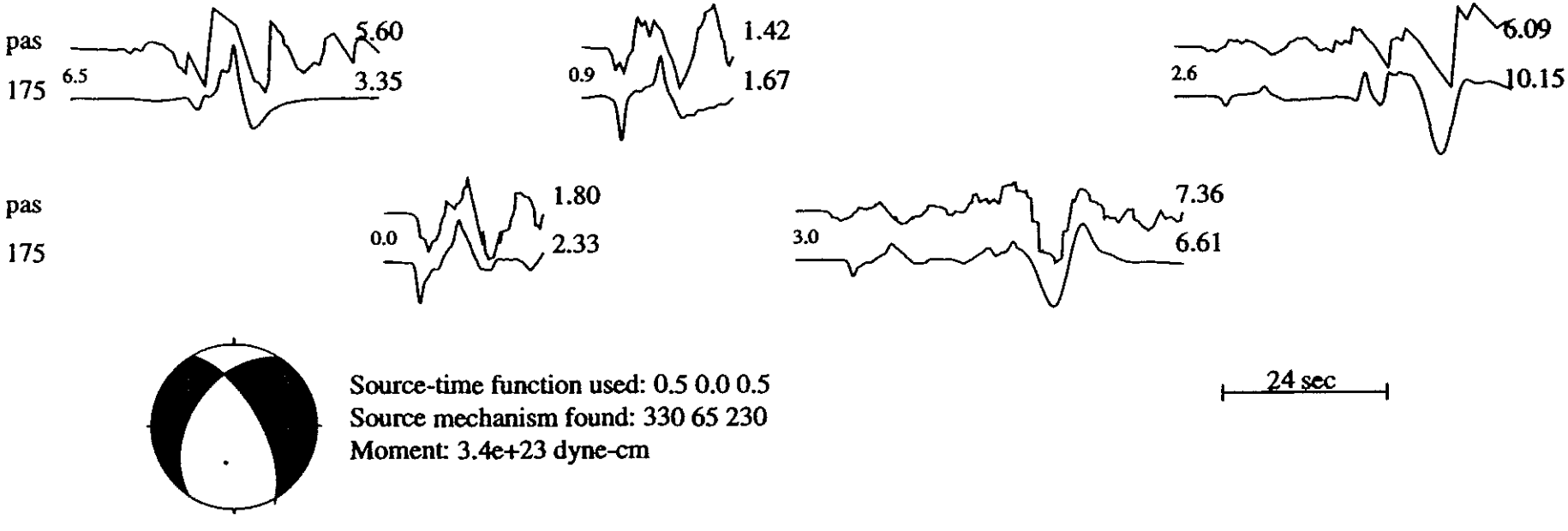
pas
175
6.5
5.60
3.35
0.9
1.42
1.67
2.6
6.09
10.15
pas
175
0.0
1.80
2.33
3.0
7.36
6.61
Source-time function used: 0.5 0.0 0.5
Source mechanism found: 330 65 230
Moment: 3.4e+23 dyne-cm
24 sec

Fig 9

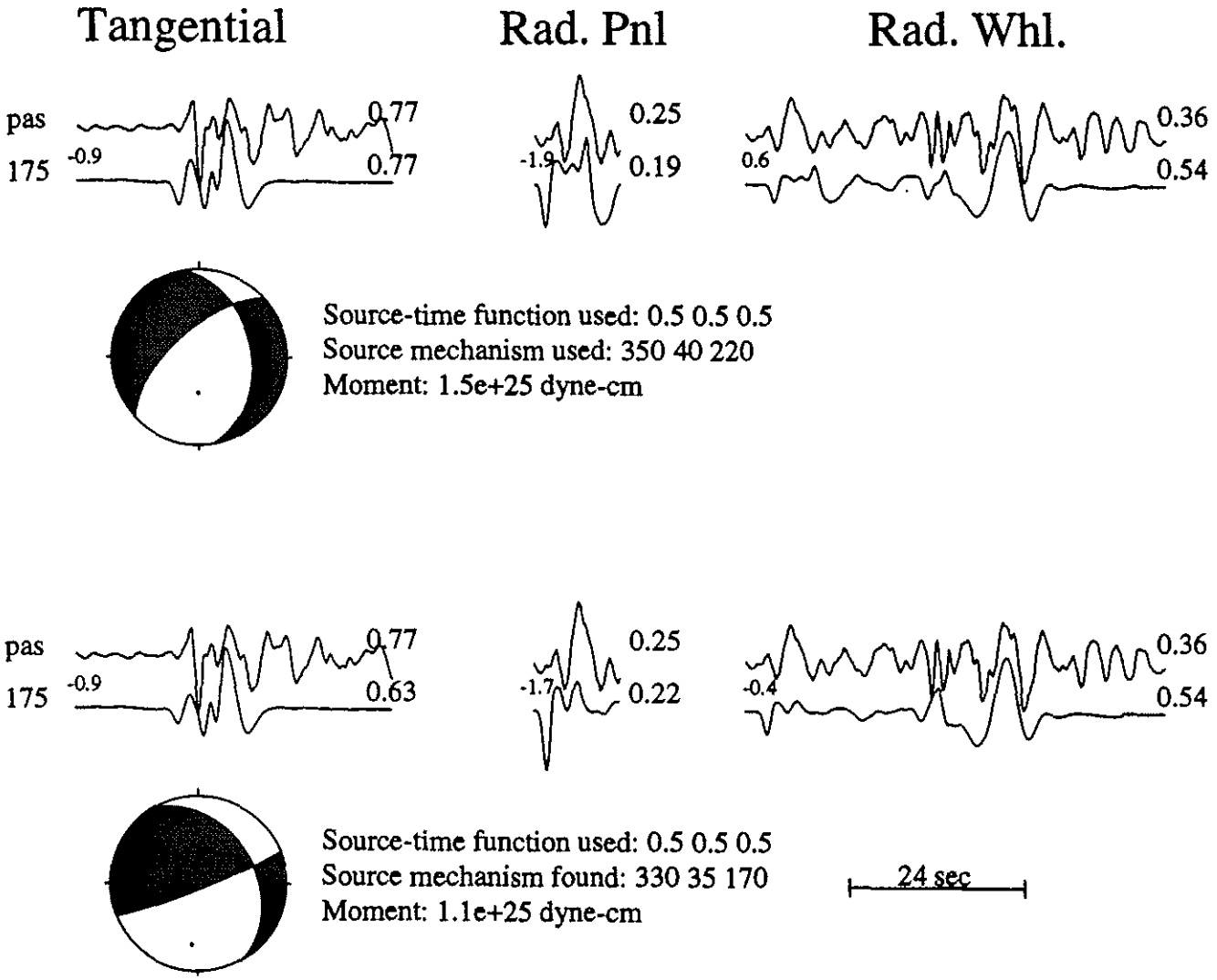
Tangential
Rad. Pnl
Rad. Whl.
pas
175
-0.9
0.77
0.77
-1.9
0.25
0.19
0.6
0.36
0.54
Source-time function used: 0.5 0.5 0.5
Source mechanism used: 350 40 220
Moment: 1.5e+25 dyne-cm
pas
175
-0.9
0.77
0.63
-1.7
0.25
0.22
-0.4
0.36
0.54
Source-time function used: 0.5 0.5 0.5
Source mechanism found: 330 35 170
Moment: 1.1e+25 dyne-cm
24 sec

Fig 10

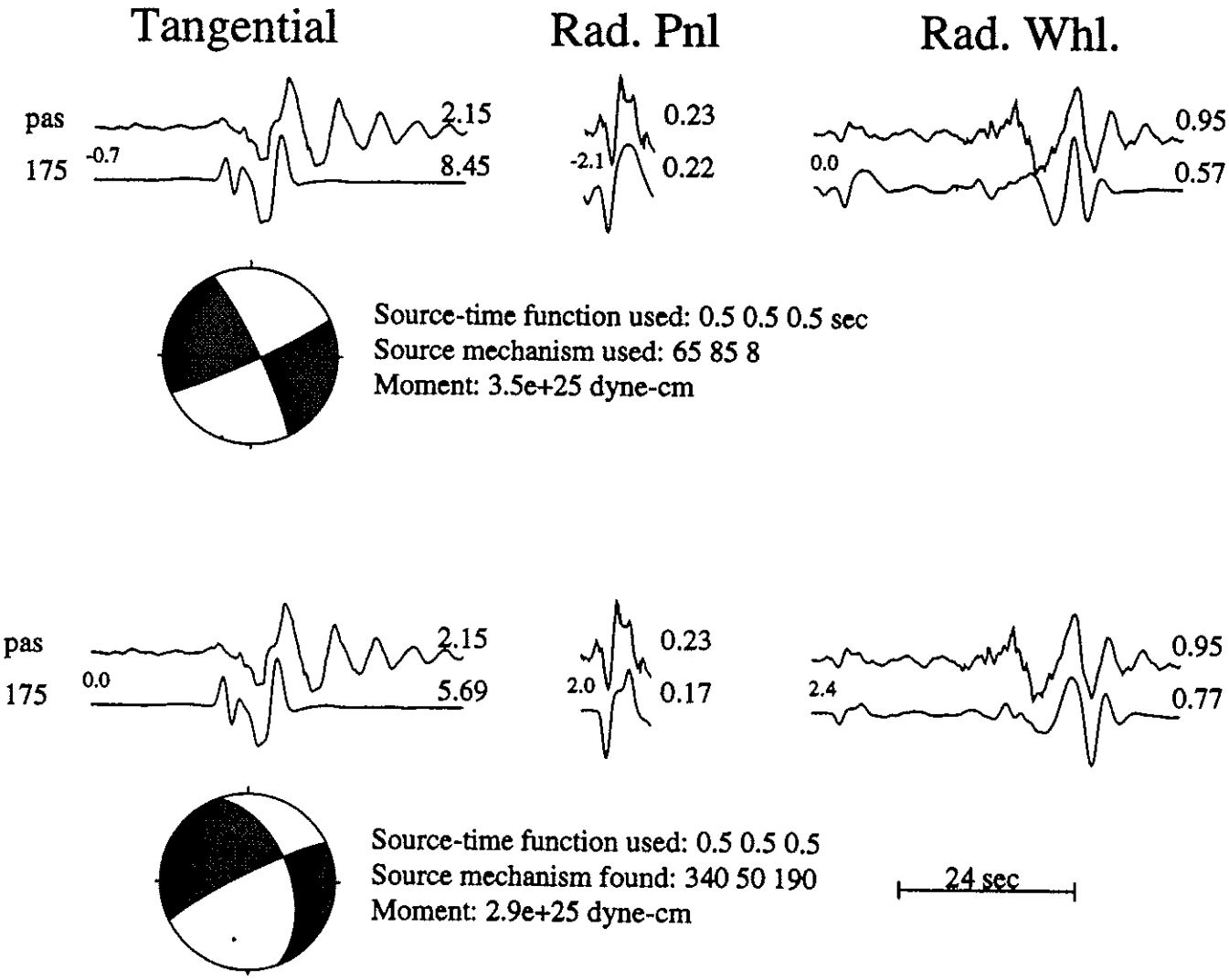
Tangential
Rad. Pnl
Rad. Whl.
pas
175
-0.7
2.15
8.45
-2.1
0.23
0.22
0.0
0.95
0.57
Source-time function used: 0.5 0.5 0.5 sec
Source mechanism used: 65 85 8
Moment: 3.5e+25 dyne-cm
pas
175
0.0
2.15
5.69
2.0
0.23
0.17
2.4
0.95
0.77
Source-time function used: 0.5 0.5 0.5
Source mechanism found: 340 50 190
Moment: 2.9e+25 dyne-cm
24 sec

fig 11

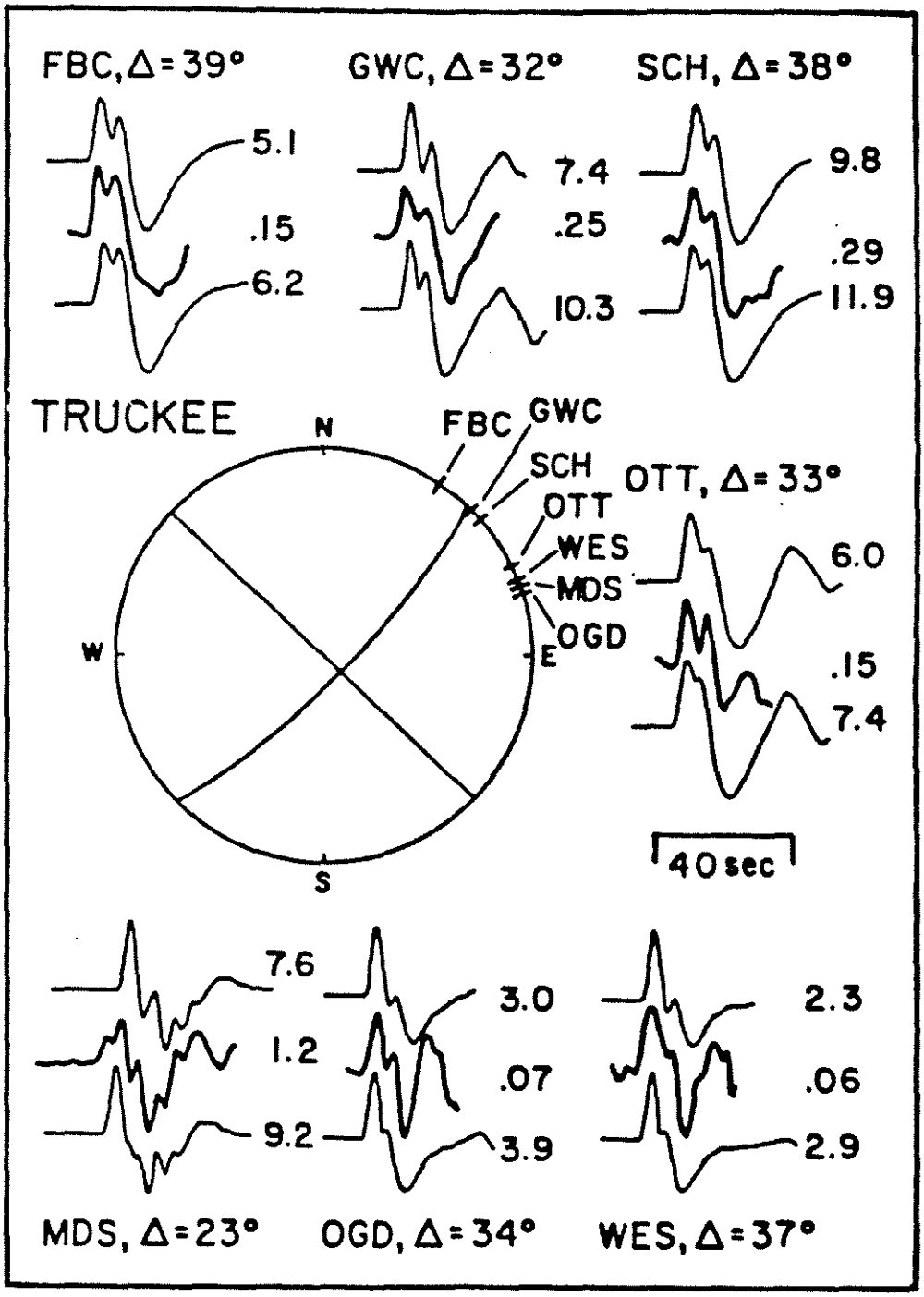
FBC, Δ = 39°
5.1
.15
6.2
GWC, Δ = 32°
7.4
.25
10.3
SCH, Δ = 38°
9.8
.29
11.9
TRUCKEE
N
W
E
S
FBC
GWC
SCH
OTT
WES
MDS
OGD
OTT, Δ = 33°
6.0
.15
7.4
40 sec
7.6
1.2
9.2
3.0
.07
3.9
2.3
.06
2.9
MDS, Δ = 23°
OGD, Δ = 34°
WES, Δ = 37°

fig 12

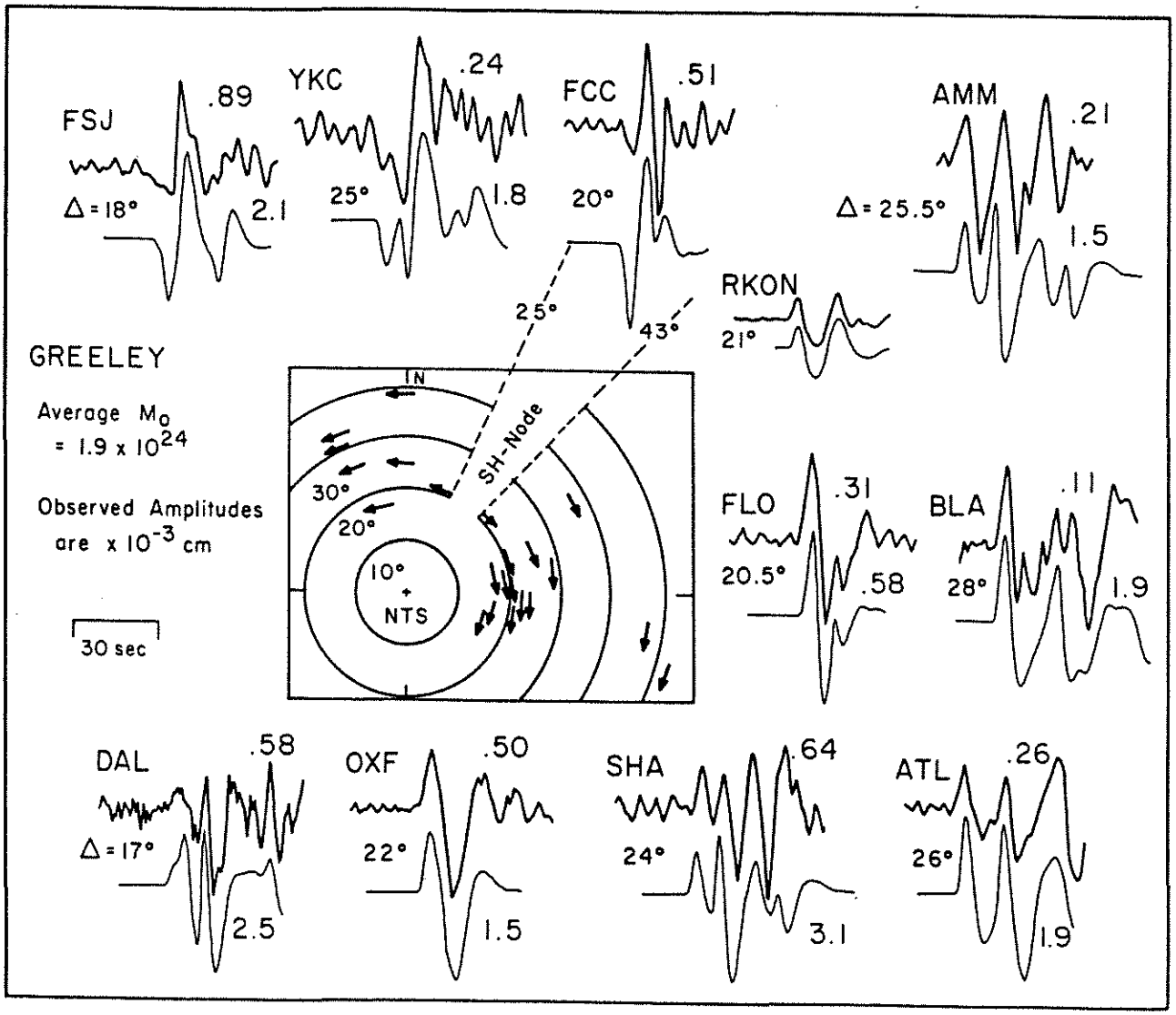

fig 13

Walker Pass 16 Sept 1962

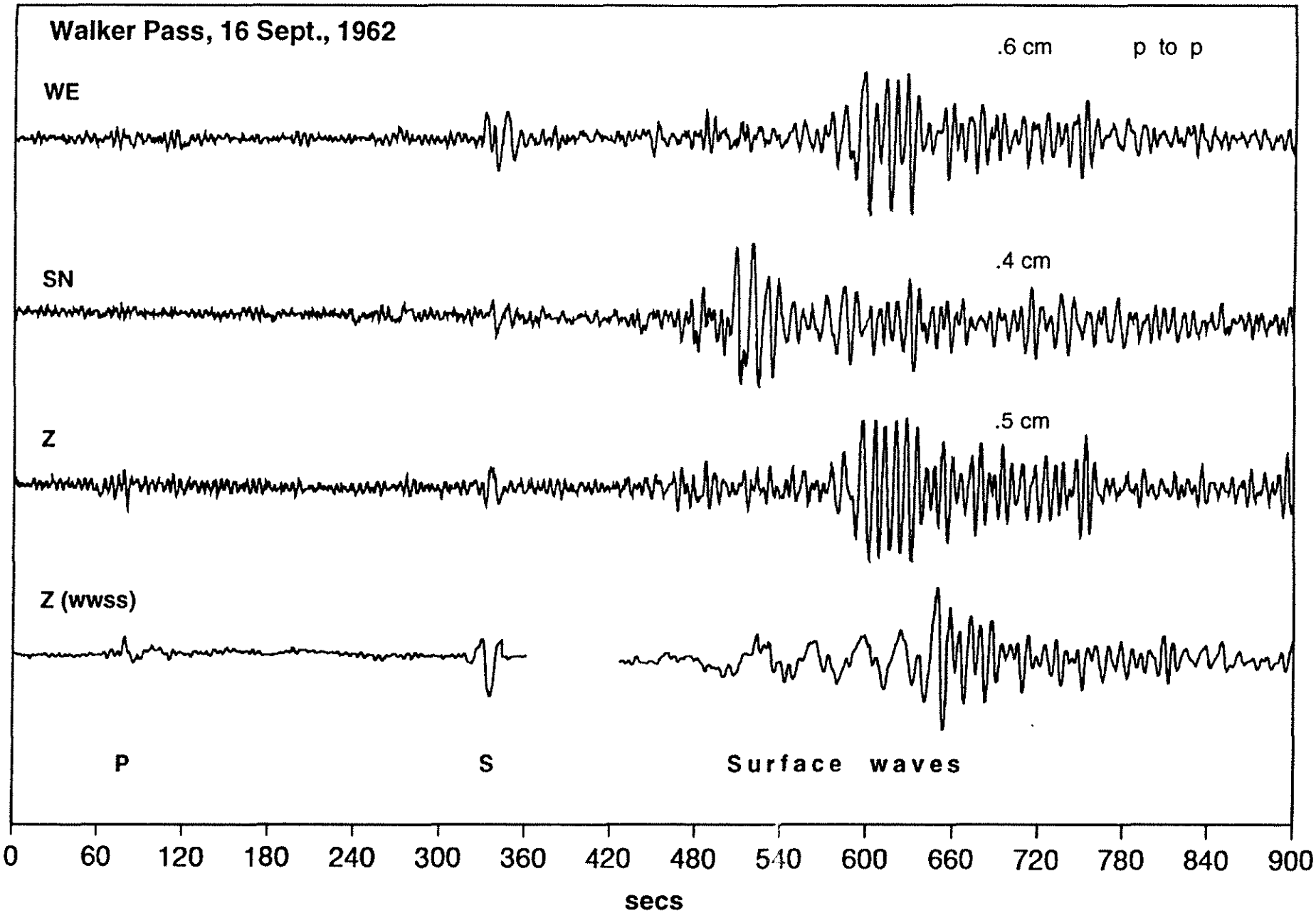
Walker Pass, 16 Sept., 1962
.6 cm
p to p
WE
.4 cm
SN
.5 cm
Z
Z (wwss)
P
S
Surface waves
0
60
120
180
240
300
360
420
480
540
600
660
720
780
840
900
secs

fig 14

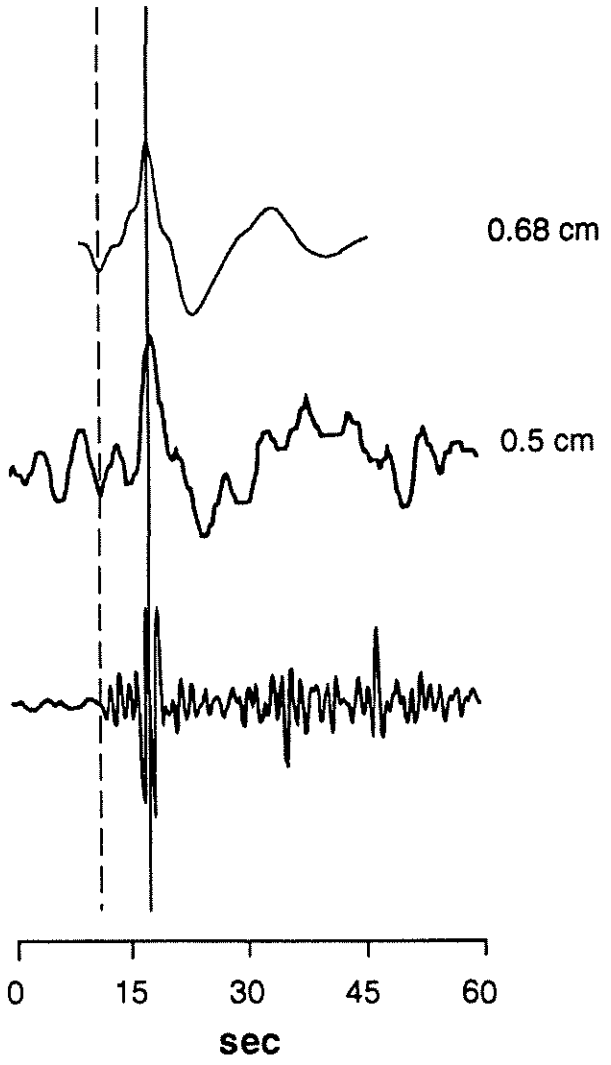

fig 15

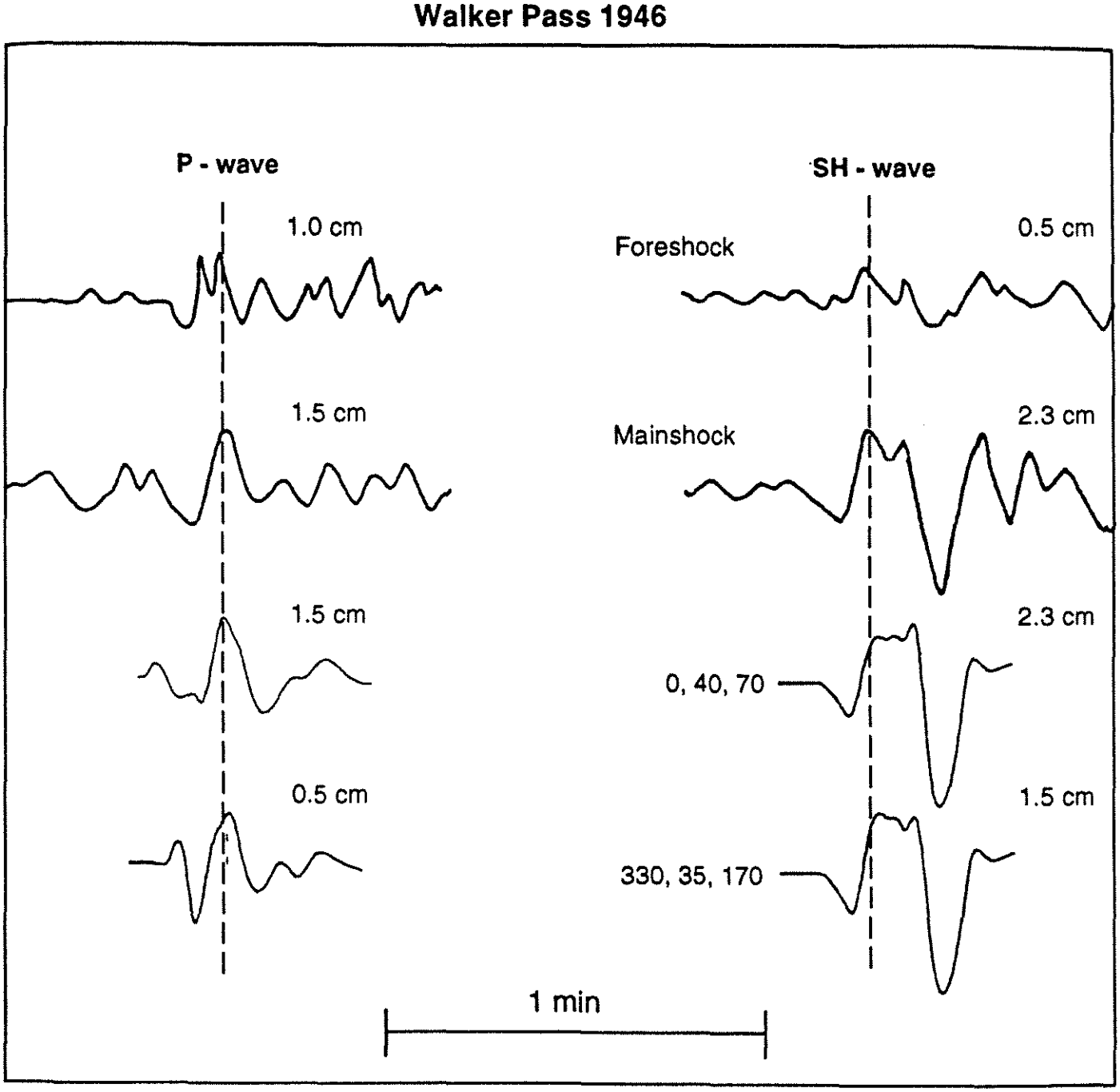
Walker Pass 1946
P - wave
SH - wave
1.0 cm
Foreshock
0.5 cm
1.5 cm
Mainshock
2.3 cm
1.5 cm
2.3 cm
0, 40, 70
0.5 cm
1.5 cm
330, 35, 170
1 min

fig 16

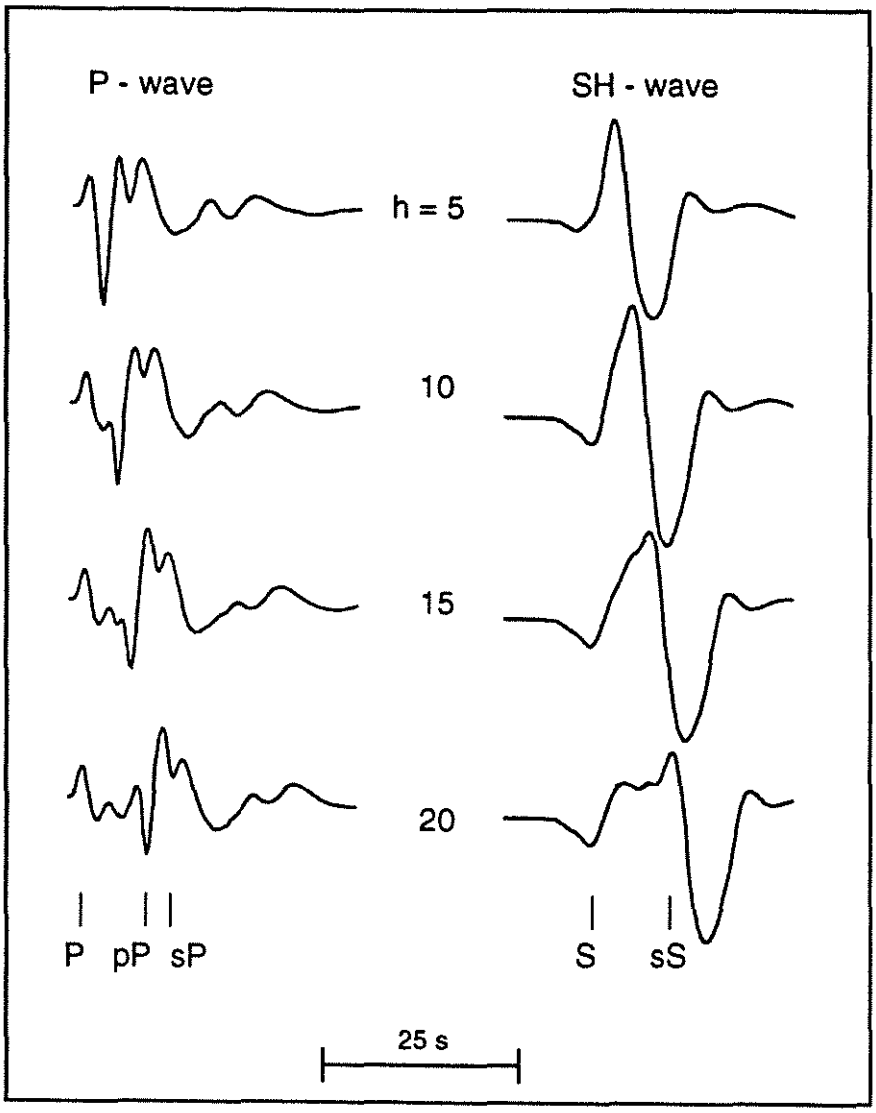

fig 17

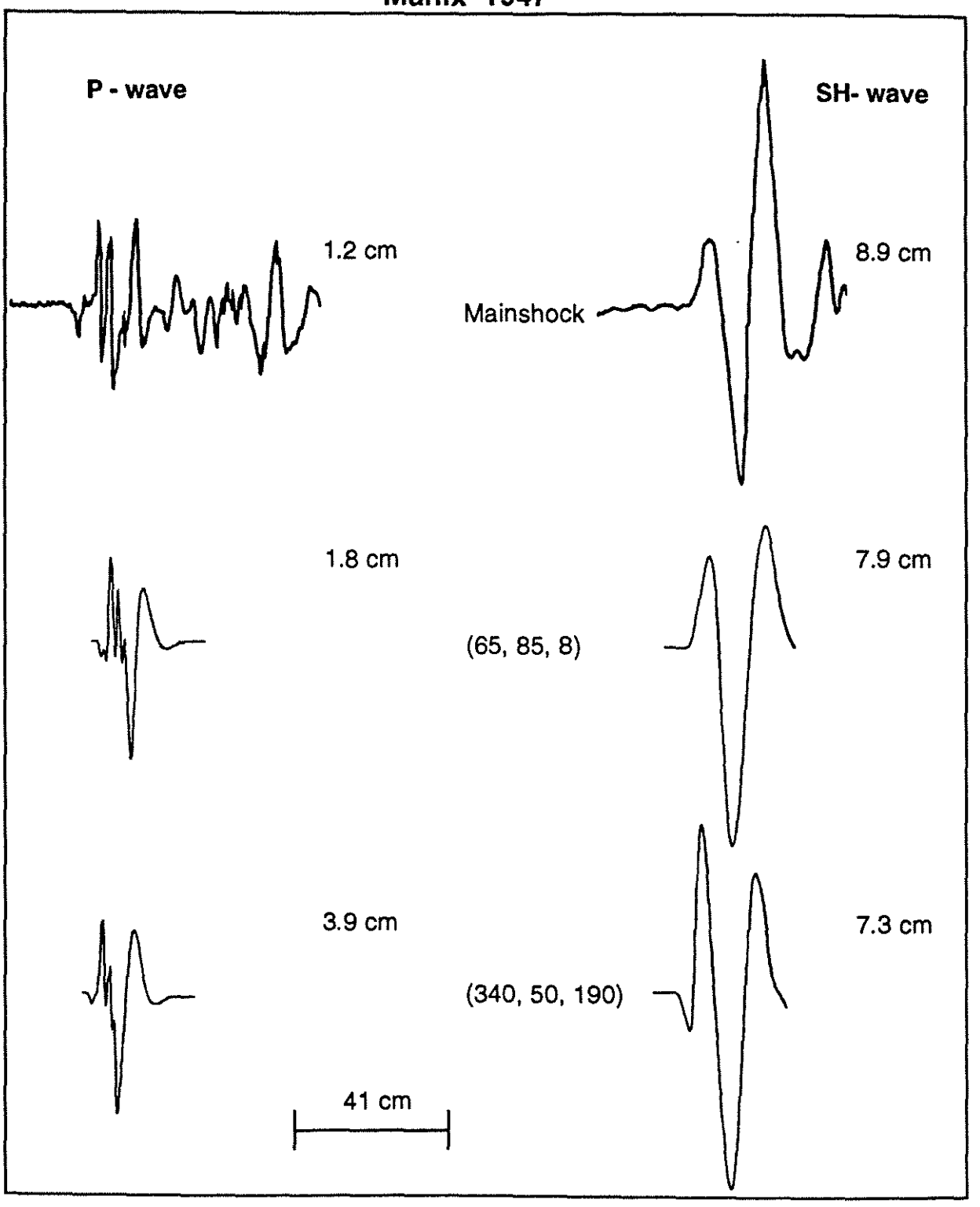
Manix 1947
P - wave
SH- wave
1.2 cm
8.9 cm
Mainshock
1.8 cm
7.9 cm
(65, 85, 8)
3.9 cm
7.3 cm
(340, 50, 190)
41 cm

fig 18